Environmental Science and Ecotechnology 27 (2025) 100614

Contents lists available at ScienceDirect

Environmental Science and Ecotechnology

journal homepage: www.journals.elsevier.com/environmental-science-and-ecotechnology/

Original Research

Real-time sludge moisture monitoring via jet imaging and deep learning

Tiefu Xu [a], Bo Zhang [a], Yue Sun [a], Man Wang [a], Yuejia Chen [a], Penghe Zhu [a], Binqiao Ren [b], Yanhong Jie [a], Guotao Wang [a,*]

[a] Heilongjiang University, Harbin, 150080, China
[b] Institute of Advanced Technology, Heilongjiang Academy of Sciences, Harbin, 150009, China

ARTICLE INFO

Article history:
Received 15 January 2025
Received in revised form
11 August 2025
Accepted 13 August 2025

Keywords:
Sludge jet characteristics
Deep learning model
Sludge moisture content
Real-time monitoring

ABSTRACT

Waste activated sludge from wastewater treatment plants poses a major environmental challenge, with its high moisture content complicating disposal and resource recovery processes across global industries. Efficient sludge management requires precise moisture monitoring to optimize treatment methods, reduce costs, and enhance outcomes such as anaerobic digestion and composting. Traditional approaches for moisture measurement are time-intensive and batch-based, while emerging techniques, such as infrared or nuclear magnetic resonance methods, suffer from inaccuracies, high costs, or limitations in real-time applications. Here we show that sludge jet characteristics, reflecting its non-Newtonian fluid properties, can be captured via high-speed imaging and analyzed with deep learning to accurately predict moisture content within 20 s. By developing a laboratory-scale system of instantaneous capturing of activated sludge jet expansion images (iCASJEI), we acquired over 11,000 jet images across 79–94 % moisture ranges and trained convolutional neural networks, with VGG-16 outperforming AlexNet and LeNet under optimized conditions (0.2 MPa pressure, 4 mm aperture), achieving 93.5 % validation accuracy at 2 % precision and 87.6 % at 1 % precision. These findings show that incorporating iCASJEI to extract non-Newtonian fluid characteristics from sludge jets with deep learning algorithms can substantially reduce testing time for sludge moisture content. This approach could also be applicable to other sectors where non-Newtonian fluid characteristics enable real-time moisture detection in viscous liquids.

1. Introduction

In 2020, the production of dry sludge in the European Union and China exceeded 13.0 million tons and 13.3 million tons, respectively. Worldwide, the production is projected to increase to 127.5 million tons by 2030, underscoring the critical necessity for the development and implementation of effective disposal technologies [1,2]. The management of this sludge constitutes approximately 30 % of the operational expenses of a typical municipal wastewater treatment plant (WWTP) [3], depending on the extent of sludge drying within the facility [4]. Drying sludge is essential to reducing moisture levels, and it greatly affects methane yield during subsequent anaerobic digestion [3,5], sludge composting efficiency [6,7], heavy metal migration during sludge incineration [8,9], and the products of sludge thermal hydrolysis [10–12].

A swift evaluation of sludge moisture levels is crucial for the effective operation of wastewater treatment processes during sludge treatment [13]. However, there is currently a lack of a real-time method for monitoring sludge moisture content, highlighting a research gap in the sustainable management of sludge.

The moisture content of sludge is related to its rheological characteristics, including thixotropy, pseudoplastic fluid behavior, and shear-thinning properties [14–16]. There are four commonly employed methods for measuring the moisture content of sludge. First, the thermal drying method is a widely utilized technique that is favored for its simplicity and accuracy in quantifying sludge moisture content; however, it is time-consuming, often necessitating more than 4 h for completion [17,18]. Second, the infrared

* Corresponding author.
E-mail address: wanggt@hlju.edu.cn (G. Wang).

https://doi.org/10.1016/j.ese.2025.100614

method, although quick, is susceptible to inaccuracies when the samples are small and have a high moisture content. Nonetheless, it can initiate transformation and carbonization within minutes, greatly surpassing the hours needed by traditional methods [19]. Third, time domain reflectometry, often used for real-time moisture content assessment during composting, encounters obstacles due to its sensitivity to temperature rises and the conductivity limitations of sludge [20,21]. Finally, low-field proton nuclear magnetic resonance (^{1}H NMR) spectroscopy, which measures sludge moisture by correlating NMR signal peaks with hydrogen protons, offers significant advantages in analyzing water distribution. However, its efficacy is compromised by interference from various sludge types and reagents, in addition to prohibitive costs, which restrict its application for moisture testing [22–24]. We quantified the non-Newtonian fluid properties of sludge and integrated machine learning and sludge recognition technologies to develop a novel approach that addresses the shortcomings of existing methods for detecting sludge moisture content.

A correlation can be established between the fluid behavior of sludge and its moisture content based on its rheological properties. Sludge behaves as a Newtonian fluid when its moisture content exceeds 97 % [25]. Conversely, it exhibits non-Newtonian fluid characteristics when the moisture content falls below 97 % [26]. This non-Newtonian behavior includes shear thinning (moisture content between 94 % and 96 %) [27], thixotropy (moisture content between 93 % and 85 %) [28], and viscoelasticity (moisture content below 85 %) [29]. Through this analysis, a theoretical evaluation of the rheological characteristics of sludge enables an estimation of its moisture content. For example, Wang et al. examined the rheological properties of three different types of sludge during the dewatering process, observing variations in rheological properties with varying moisture contents. Their study ultimately predicted the rheological behavior of sludge, with moisture contents ranging from 70 % to 85 % [30].

Moisture content in sludge is hypothesized to be assessable through jet images of mixed liquor (JIML), which leverage the analysis of non-Newtonian fluid jets. These jets offer high reproducibility, low operational complexity, and rapid assessment. JIML shows considerable promise for evaluating the moisture content of sludge due to its efficiency and reliability. The primary challenge resides in the capability to conduct large-scale JIML for model training and validation. In this study, we present a deep learning method based on jet image features. We established a sewage jet system and compared the results under various conditions with different model parameters. The aim is to establish a fast, real-time method for measuring sludge water content using instantaneous capture of activated sludge jet images (iCASJEI). Our results indicate a correlation between the non-Newtonian fluid properties of sludge and its moisture content.

2. Materials and methods

2.1. Sludge and sample preparation

The moisture content data used for training the models were obtained from samples collected at three WWTPs. These WWTPs manage daily sewage treatment volumes of approximately 50,000, 100,000, and 150,000 tons, resulting in dewatered sludge outputs of 160, 280, and 450 tons, respectively. Each WWTP operates under a cyclic activated sludge system, with sludge dewatering facilitated using belt-type filters following the addition of polyacrylamide. The annual average moisture content of the processed sludge is 81–87 %.

Sludge samples collected from sludge treated by filter presses or dehydrators in sewage plants were promptly placed in ice-filled containers and transported to a cold storage room maintained at 4 °C within a 4-h period, where they remained until required for use. The fundamental properties of the sludge, including moisture content, pH, the ratio of total suspended solids to volatile suspended solids (VSS/TSS), conductivity, median particle diameter ($d_{0.5}$), and apparent viscosity, were assessed following established standard methods [31] (Table 1). For indicators such as moisture content, the measurement accuracy was precisely controlled within a specific range (e.g., moisture content accuracy of ±0.1) and determined using methods such as heating and drying. The pH was measured using a laboratory pH meter. For VSS/TSS, with measurement methods involving heating and drying. Conductivity was measured with an accuracy of ±0.1 using a conductivity meter. Median particle size (±0.1) was measured using a laser particle analyzer, and apparent viscosity (±0.5) was measured using a rotational viscometer.

We utilized deionized water to prepare the sludge samples, which exhibited moisture contents ranging from 87 % to 94 %. To obtain sludge samples with a reduced moisture content (79–86 %), a low-temperature (60 °C) drying process was employed for varying durations. Consequently, 16 distinct sludge samples with moisture contents ranging from 79 % to 94 % were successfully prepared, with each sample differing by 1 % in moisture content, thereby creating a continuous concentration gradient. Subsequently, the actual moisture content of each sludge sample was validated using conventional methods, with discrepancies from the target moisture content remaining below a specified threshold (5 ‰).

2.2. Instantaneous capturing of JIML

We developed a laboratory-scale apparatus designed to capture images of sludge jets. The apparatus comprises four primary components: a stabilized gas supply unit, a stamping unit, a fluidic element, and an image acquisition unit (Fig. 1 and Table 2). The operation of the entire process of the JIML test consists of ten steps: (1) activate the air compressor and adjust the pressure regulator until a stable reading is achieved; (2) load the prepared sludge sample into the jet cavity and agitate it thoroughly using an ultrasonic oscillator for uniformity; (3) assemble and seal the nozzle before positioning it upside down beneath the shockproof table; (4) ensure consistent illumination of 5120 ± 100 lux beneath the table using a fill light; (5) capture image data with a high-speed camera at 260 frames per second; (6) remove the sealing piece from the jet cavity after the high-speed camera is activated; (7) initiate the stamping system with compressed air from the air compressor driving the stamping bolt downward; (8) initiate the jet flow by sludge within the cavity extruded downward through the nozzle; (9) reset the cylinder automatically and deactivate the high-speed camera upon the jet flow completely; and (10) edit and save the raw data (Supplementary Table S1). The reaction chamber strictly adheres to the standardized pretreatment protocol, involving sequential high-pressure water jet rinsing and ultrasonic oscillation cleaning. The statistical analysis of the raw dataset indicates that the residual rate consistently remains below 0.1 %, confirming its negligible impact on the experimental outcomes.

2.3. Image processing and dataset construction

Following the completion of the experiment, the raw data were systematically annotated, cropped, and manually filtered to eliminate blurred and invalid frames from the original sludge jet feature videos, thereby constructing a comprehensive video dataset. Subsequently, a custom Python program was employed to extract images from this dataset at a rate of one image every ten

Table 1
Characteristics of activated sludge from different factories.

Indicator	Moisture content (%)	pH	VSS/TSS	Conductivity (μs cm^{-1})	$d_{0.5}$ (μm)	Apparent viscosity (Pa s)
WWTP #1	86.8 ± 0.5	7.31	0.30	945.2 ± 9.4	93.8 ± 1.1	17.1 ± 0.3
WWTP #2	85.3 ± 0.5	6.93	0.30	892.5 ± 17.7	108.8 ± 2.2	15.1 ± 0.4
WWTP #3	84.5 ± 0.7	7.22	0.31	960.3 ± 9.4	126.4 ± 2.4	14.1 ± 0.3
Huadu, Beijing	89.3 ± 0.9	6.84	0.31	1035.8 ± 10.2	101.3 ± 2.0	26.7 ± 0.3
Daoxiangcun, Beijing	82.9 ± 0.8	6.91	0.35	1644.7 ± 33.1	98.5 ± 1.7	26.2 ± 0.5
Buji, Shenzhen	81.4 ± 0.5	6.94	0.33	1376.3 ± 34.4	98.7 ± 2.2	26.9 ± 0.4
Xili, Shenzhen	75.5 ± 0.9	6.53	0.35	1740.2 ± 50.3	95.9 ± 0.9	27.5 ± 0.3
Binhe, Shenzhen	81.3 ± 0.8	6.42	0.39	1580.3 ± 34.8	91.3 ± 0.9	26.9 ± 0.4

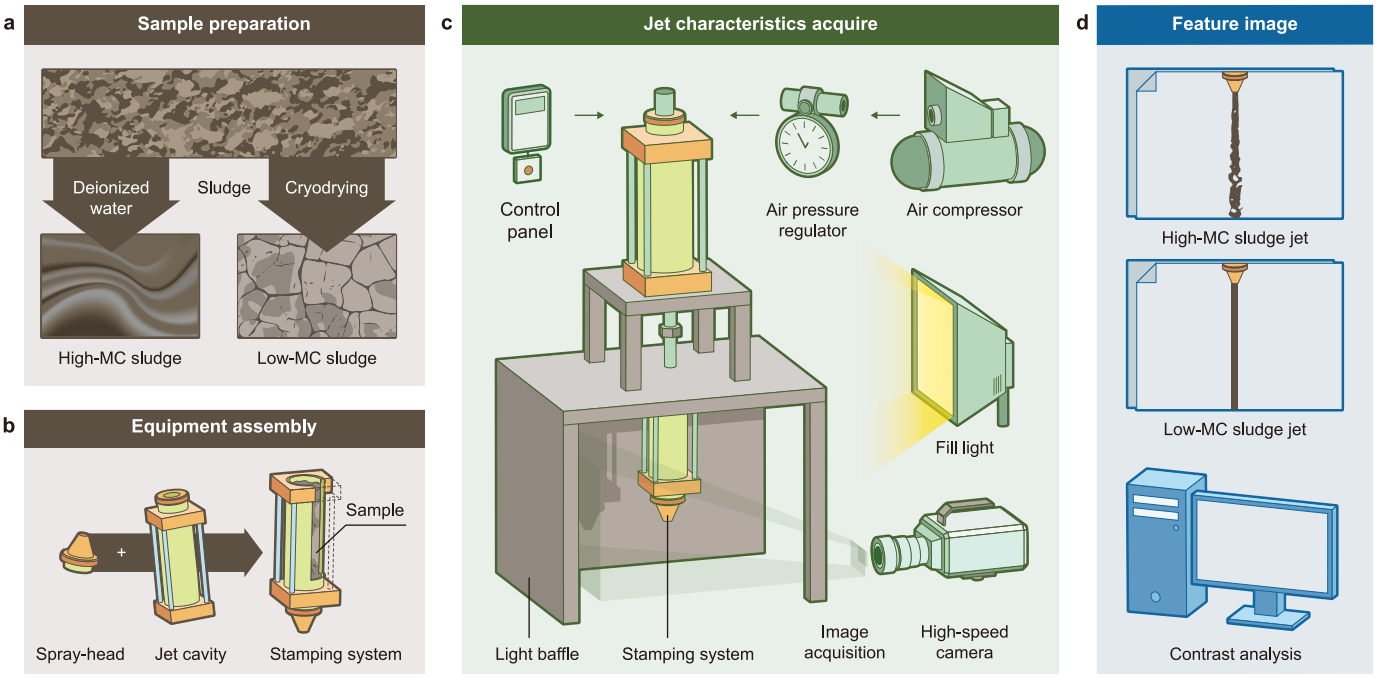

Fig. 1. Flowchart illustrating the process of the instantaneous capturing of activated sludge jet expansion images and image acquisition. MC: moisture content.

Table 2
Main structural units of the jet images of mixed liquor test device: parameters and functions.

System	Component	Parameter	Function
Stabilized gas supply unit	Air compressor, pressure gauge, air pressure regulator, and air pipeline	Pressure range: 0.0–0.6 MPa	Power source for the equipment, and provides stable and adjustable pressurized air to the stamping system
Stamping unit	Pressure gauge, cylinder, manual switch, automatic control module, and stamping bolt	Pressure load and output: 0.0–1.0 MPa	Pressure output unit that delivers pressurized air from the stabilized gas supply system through a rigid body output
Fluidic element	Jet cavity, seal, and nozzle	Capacity: 300 mL; Nozzle aperture: 1–5 mm	Sludge storage, jet characteristic enhancement, and generation unit
Image acquisition unit	High-speed camera, fill light, light frame, shading board, background board, and shockproof table	Video resolution: 640 × 360; Frame rate: 260 fps; illuminance of fill light: approximately 5120 ± 100 lux	Provides illumination and captures the sludge jet characteristic image data

frames (see Fig. 2). The data were subsequently categorized into four distinct datasets following the requirements for model construction:

(1) Model selection dataset (2050 images). This dataset comprises images depicting sludge exhibiting moisture content ranging from 87 % to 94 %, obtained under a jet pressure of 0.2 MPa and a jet diameter of 4 mm. It is used to determine the most effective model for predicting moisture content.

(2) Jet pressure comparison dataset (2412 images). This dataset, comprising images of sludge with moisture content ranging from 87 % to 94 % under jet pressures of 0.2, 0.4, and 0.6 MPa, was employed to assess the impact of jet pressure on moisture content prediction.

(3) Jet diameter comparison dataset (3231 images). This dataset includes images with varying sludge moisture content, ranging from 91 % to 94 %, which helps determine the optimal jet diameter conditions.

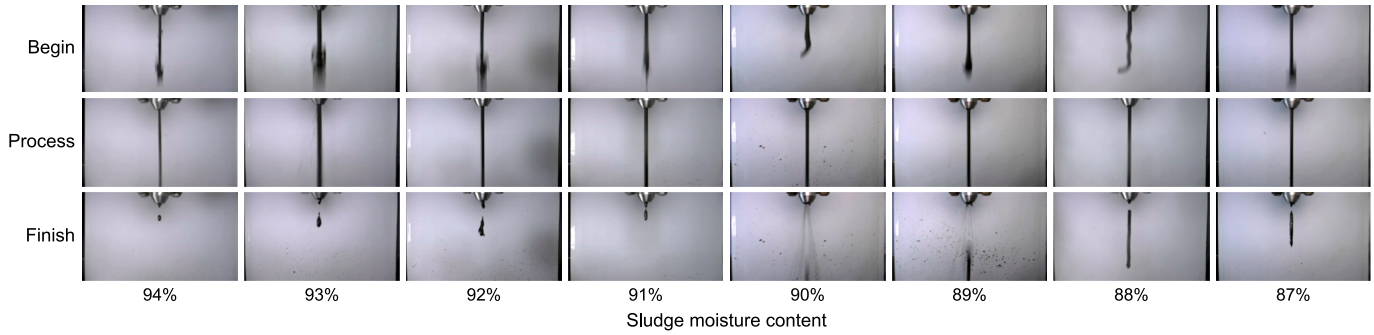

Fig. 2. Jet images of sludge with varying moisture content at a pressure of 0.2 MPa and a jet diameter of 4 mm. The setup uses hoods, splash guards, and white illumination to stabilize the light field and enhance image quality with a white background. Two light-emitting diodes provide illumination with algorithmic interference mitigation.

(4) Sludge moisture content prediction dataset (11,641 images). This extensive dataset encompasses images obtained from all validated experimental conditions.

To ensure the validity of the model parameters following the training phase and to evaluate the model's performance in practical applications, the dataset was partitioned into training, validation, and test subsets in a ratio of 60:20:20. The training and validation subsets were employed to enhance the model's predictive accuracy regarding sludge moisture content and to optimize the model parameters. Conversely, the test subset, which was not used during model training, was exclusively designated for assessing the predictive performance of a trained convolutional neural network (CNN) on unlabeled actual sludge jet images.

Hyperparameter selection is crucial for model convergence, generalization, and performance in deep learning training. In this study, we used stochastic gradient descent with an initial learning rate of 0.0005 and a momentum of 0.8 to accelerate optimization and avoid local minima. Regularization, specifically L2 regularization, mitigates overfitting by penalizing excessively large model weights (Supplementary Text S1). In this study, weight decay was set to 5×10^{-4} to implement L2 regularization effectively. The learning rate was scheduled using StepLR, halving every ten epochs (gamma = 0.5) to stabilize later training stages. The loss function was cross-entropy loss, which is suitable for multiclass tasks. The model was trained for 100 epochs to fully capture spatiotemporal features.

2.4. Prediction models

2.4.1. Convolutional neural network models

Three CNN models were employed for image classification: LeNet [32], AlexNet [33], and VGG-16 [34]. Following the training process with a uniform dataset, the model that exhibited the optimal performance was chosen for further examination.

LeNet, proposed in 1998, is the most classic shallow CNN with a four-layer CNN structure [35]. It comprises three convolutional layers formed by 5×5 kernels, two pooling layers, and a single fully connected layer. Employing the Sigmoid function ($f(x) = (1 + e^{-x})^{-1}$) as the activation function enhances its capability for complex classification [36]. AlexNet, introduced in 2012 and building upon the foundation of LeNet, marks the transition from shallow to deep CNNs [37]. It features an eight-layer CNN comprising five convolutional layers, three pooling layers, and three fully connected layers. The model's increased depth and adoption of rectified linear unit (ReLU) as the activation function contribute to improved performance and adaptability in classification tasks. VGG-16, recognized for its simple and uniform structure, emerged in 2014 [38]. This deep CNN comprises 16 layers, including 13 convolutional layers and three fully connected layers [39]. The network's depth and the uniform use of 3×3 convolutional kernels enhance its performance, reducing computational complexity and enhancing efficiency with increased depth [40].

2.4.2. Model comparison

Initially, a comparative analysis was conducted among three CNN models, and the one with the best performance was selected as the foundation for the development of subsequent predictive models. Subsequently, based on this optimal model, six identical models were created. These models were individually trained on datasets specific to jet pressure or diameter to determine the optimal parameters associated with jet pressure and diameter. Ultimately, a dataset containing the most relevant data for recognition was used to train the model to predict the moisture content of sludge.

The model development process was conducted using PaddlePaddle [41], while data analysis and visualization were facilitated by Matplotlib [42], NumPy [43], and Pandas [44]. LeNet and AlexNet retained their original architectures, whereas the final layer of VGG-16 was eliminated to better align with the task requirements. The images used for model training retained their original formats, with modifications made solely to comply with the input specifications of each respective model. During the training phase, the optimal number of epochs was determined for each model, with VGG-16 demonstrating superior performance at the 50-epoch interval, surpassing both AlexNet and LeNet in terms of the number of epochs required. This customized approach, particularly the removal of the final layer in VGG-16, significantly mitigated the complexity associated with model deployment.

2.4.3. Model evaluation

The model's predictions were utilized to determine the moisture content of the sludge. Accuracy, defined as the ratio of correct predictions (the sum of true positives and true negatives) to the total number of predictions, was used to assess the model's classification efficacy.

The loss function serves as a parameter to assess the disparity between the model's predictions and the actual values; a lower loss function signifies superior model performance. The confusion matrix provides a visual representation of the model's prediction results in comparison to the actual values. Each column denotes a predicted category, wherein the values specify the number of true instances that were predicted to belong to that category, while the total reflects the model's predictions for that particular category. Conversely, each row signifies the true classification of the data,

with the total indicating the number of instances of true data.

The model's performance was evaluated using the following metrics: validation accuracy, validation loss, and test accuracy. Validation accuracy assesses the adequacy of the model parameters, whereas test accuracy measures the model's effectiveness in predicting the actual moisture content of sludge using images from the testing phase set.

3. Results and discussion

3.1. Optimal model selection

We conducted a comprehensive performance evaluation of the three models, considering rationality and actual test outcomes, to ascertain the most effective predictive model.

VGG-16 was found to be the optimal model for predicting sludge moisture content. Higher validation accuracy values indicate more reasonable model parameter settings. The validation accuracies for VGG-16, AlexNet, and LeNet were 99.3 %, 82.4 %, and 90.2 %, respectively (Table 3), indicating that VGG-16 and LeNet performed better in predicting sludge moisture content. Regarding validation loss, lower values indicate fewer prediction errors during model operation on the validation dataset, resulting in better performance. We found that VGG-16 had the lowest prediction loss (5.8 %), while AlexNet and LeNet displayed loss levels of 15.5 % and 38.4 %, respectively (Table 3). Smoothness in the training process curves is also important. The training curves for both VGG-16 and AlexNet demonstrated notable smoothness (Fig. 3).

In terms of testing accuracy, higher values indicate superior performance in practical testing. The post-trained VGG-16 model achieved an accuracy of 96.7 % on 793 randomly chosen unlabeled images from the model selection dataset, surpassing AlexNet (63.4 %) and LeNet (73.7 %) (Table 4). To further verify the model's focus on key features in jet images, we used Grad-CAM to visualize the VGG-16 model's predictions. Supplementary Fig. S1 presents four randomly selected visualization maps of different moisture contents. The Grad-CAM significance maps highlight the areas the model prioritizes during moisture prediction. For jet images, the model emphasizes the edge sharpness and dispersion patterns of the jet stream, directly reflecting the moisture distribution during ejection. The areas highlighted in red and yellow show a strong model response to the core and surrounding diffusion regions of the jet. This supports the significant differences in jet images and demonstrates the model's ability to capture key visual features for moisture prediction, thereby improving the reliability and interpretability of the predictions.

We conducted ten experiments for each of the three models (Table 4). Based on the experimental data, we carried out comparative statistical analyses between VGG-16 and the other two models (AlexNet and LeNet) to evaluate the significance and practical differences in their performance. The analysis revealed a highly significant difference between VGG-16 and AlexNet, with a p-value of less than 0.001, effectively ruling out the possibility of random errors. The Cohen's d effect size was 20.90, where a value of $d > 0.80$ is typically considered large. This indicates a substantial practical difference, consistent with situations in which one machine learning model significantly outperforms another. VGG-16 achieved a mean accuracy of 95.6 %, which is markedly higher than AlexNet's 64 %.

Notably, even when accounting for random variations across the ten experiments, VGG-16's lowest accuracy (94.6 %) still exceeded AlexNet's highest accuracy (67.9 %). Similarly, the difference in test accuracy between VGG-16 and LeNet was also extremely significant, with the p-value less than 0.001 and a Cohen's d of 24.5. This again signifies a very large practical difference. VGG-16's mean accuracy of 95.6 % was significantly higher than LeNet's 73.3 %. Even considering random fluctuations, VGG-16's lowest accuracy (94.6 %) was much higher than LeNet's highest accuracy (74.9 %). In summary, VGG-16 demonstrated a significant performance advantage over both AlexNet and LeNet. This conclusion is supported by strong statistical evidence and large practical differences, further confirming the superior performance of VGG-16.

Table 3
Comparison of results obtained by three conventional neural network models trained on the same dataset of 2050 sludge jet images at 87–94 % moisture content, classified into eight categories with a 1 % gradient difference.

Model	Validation accuracy	Validation loss	Test accuracy
VGG-16	99.3 %	5.8 %	96.7 %
AlexNet	82.4 %	15.5 %	63.4 %
LeNet	90.2 %	38.4 %	73.7 %

3.2. Feasibility test

We found an exponential correlation between the sludge moisture content and the apparent viscosity of the sludge, particularly as the moisture content decreased from 94 % to 87 % (Supplementary Fig. S2). When the moisture level falls to 86 % or lower, the rate of change in apparent viscosity slows down after the heat treatment process. Subsequently, it gradually reverts to an exponential pattern as moisture content decreases, aligning with prior research findings [45,46]. A linear correlation was observed between the sludge moisture content and conductivity (Supplementary Fig. S2). Below a moisture content of 94 %, conductivity exhibited a declining trend with decreasing moisture content, consistent with observations regarding sludge impedance fluctuations by Ségalen et al. [47]. These findings suggest that the apparent viscosity and conductivity variations observed in the sludge samples obtained after dehydration and reconstitution closely resemble those of directly dewatered sludge. This indicates the feasibility of using reconstituted sludge for experimental purposes, offering a viable alternative approach.

3.3. Impact of pressure and nozzle diameter

We found that nozzles with diameters of 1 and 2 mm were insufficient for spraying when the moisture content fell below a certain threshold of 93 % (Fig. 4). When the moisture content falls below 90 %, the sludge viscosity demonstrates an exponential increase, while the electrical conductivity progressively decreases with diminishing moisture content, collectively leading to recurrent nozzle clogging during operation with 3 mm diameter nozzles. The use of larger orifice plates may contribute to a diminished stability of the sludge jet and an expanded dispersion area, ultimately leading to suboptimal performance. Conversely, the 4 mm nozzle exhibited enhanced jet performance under equivalent pressure conditions. It is important to note that high-pressure processes do not necessarily yield improvements in recognition rates; rather, within the low moisture content spectrum, such processes may reduce image recognition efficiency. Consequently, optimal experimental conditions were established using a pressure of 0.2 MPa and a nozzle diameter of 4 mm.

3.4. Selection of jet pressure ratios

We employed the VGG-16 model to develop three jet pressure selection models: Model 1 (0.2 MPa), Model 2 (0.4 MPa), and

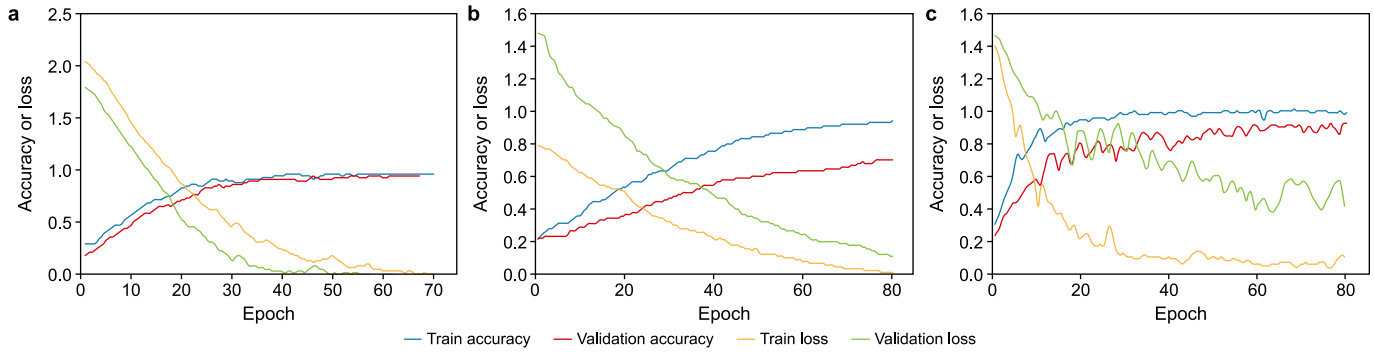

Fig. 3. Accuracy and loss function values of the training and validation sets during the training process for three models: **a**, VGG-16 model; **b**, AlexNet model; **c**, LeNet model.

Table 4
Statistical significance of accuracy from ten experimental validations for VGG-16, AlexNet, and LeNet Models.

Model	1	2	3	4	5	6	7	8	9	10
VGG-16	95.2	97.4	96.7	96.6	96.0	95.0	95.5	94.8	94.6	95.1
AlexNet	62.8	64.3	63.4	67.9	61.9	61.2	64.1	65.0	63.9	65.9
LeNet	73.4	72.7	73.7	72.8	72.4	72.5	74.9	73.7	72.9	74.7

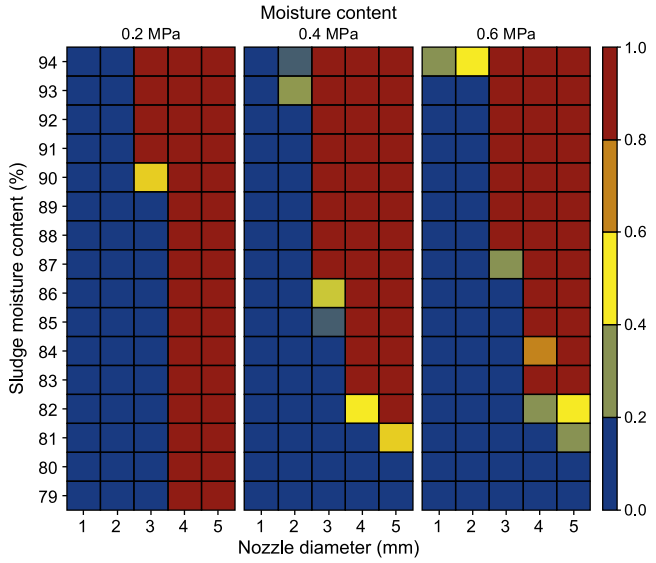

Fig. 4. Jet occurrence under experimental conditions. Evaluated pressure (0.2–0.6 MPa), nozzle diameter (1–5 mm), and moisture content (79–94 %). Blue: too small to spray; yellow: clogs; red: best performance.

Model 3 (0.6 MPa). These models were designed to predict image data under three distinct pressure conditions (0.2, 0.4, and 0.6 MPa, respectively) with a target precision of 1 % across eight categories, each representing a 1 % increment within the range of 87–94 %.

The analysis revealed that all three models exhibited high validation accuracy and low validation loss values across various pressure conditions (Table 5). Notably, the dataset for Model 1 (0.2 MPa) achieved the highest validation accuracy of 99.3 % and the lowest validation loss of 5.8 %, thereby slightly surpassing the performance of the other models. Furthermore, throughout the

Table 5
Comparison of results obtained from three deep learning models trained on a dataset of 2412 sludge jet images at 87–94 % moisture content, classified into eight categories with a 1 % gradient difference.

Model	Validation accuracy	Validation loss	Test accuracy
Model 1 (0.2 MPa)	99.3 %	5.7 %	96.7 %
Model 2 (0.4 MPa)	96.8 %	10.5 %	89.3 %
Model 3 (0.6 MPa)	92.6 %	19.0 %	83.2 %

training process, all three models displayed relatively smooth curves (Fig. 5), which indicates appropriate parameter settings and robust performance. The VGG-16 model demonstrated superior performance to the other two models (Table 5).

Ten experiments were performed for each of the three models (Table 6). Based on the experimental data, statistical analyses were conducted to compare the test accuracies of Model 1 (0.2 MPa) with those of Model 2 (0.4 MPa) and Model 1 (0.2 MPa) with those of Model 3 (0.6 MPa), assessing both significance and practical differences. Normality testing via the Shapiro–Wilk test confirmed that the data followed a normal distribution (the p-values for Model 1, Model 2, and Model 3 are 0.494, 0.460, and 0.977). Homogeneity of variance was established using Levene's test ($p = 0.249$). A one-way analysis of variance (ANOVA) revealed extremely significant performance differences among the three models, with the F-value indicating whether the differences between groups are significantly greater than random error ($F = 566.4$, $p < 0.001$). Post hoc Tukey honestly significant difference (HSD) tests revealed significant mean differences between Model 1 and Model 2 (-7.6) and between Model 1 and Model 3 (-13.5), both with p-values less than 0.050. Cohen's d analysis showed large effect sizes (10.1 for Model 1 vs. Model 2 and 14.4 for Model 1 vs. Model 3), indicating both statistical and practical significance. Overall, while Model 3 (0.6 MPa) demonstrated improved performance, Model 1 (0.2 MPa) exhibited the highest validation accuracy and lowest validation loss, showing superior stability and predictive performance, particularly under lower pressure conditions.

3.5. Selection of jet diameter ratios

We developed three models for selecting jet diameters: Model 4 (3 mm), Model 5 (4 mm), and Model 6 (5 mm), to predict the optimal conditions for experimental jet diameters. These models were trained based on a four-category prediction framework, aiming for a target precision of 1 % in the selection of the jet

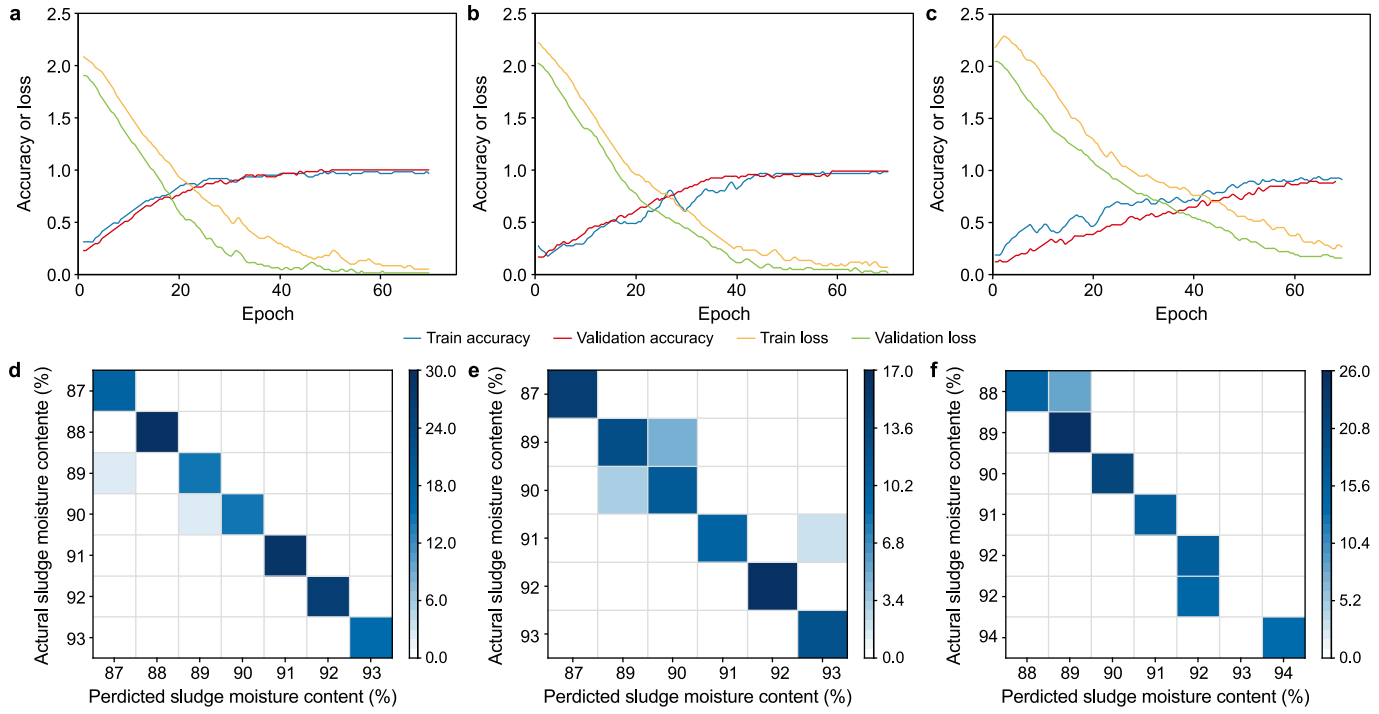

Fig. 5. a–**c,** Model training at different pressures: Model 1 (0.2 MPa, **a**); Model 2 (0.4 MPa, **b**); Model 3 (0.6 MPa, **c**). **d–f,** Confusion matrices at different pressures: Models 1 (**d**); Model 2 (**e**); and Model 3 (**f**). Model 1 at 0.2 MPa shows the lowest error rates and is optimal for prediction.

Table 6
Results of ten experimental validations for the testing accuracy of Model 1 (0.2 MPa), Model 2 (0.4 MPa), and Model 3 (0.6 MPa).

Model	1	2	3	4	5	6	7	8	9	10
Model 1 (0.2 MPa)	96.1	97.1	95.8	96.9	97.0	96.4	95.7	97.6	96.2	97.2
Model 2 (0.4 MPa)	88.7	90.2	89.0	88.0	89.6	88.3	90.0	89.4	87.9	89.6
Model 3 (0.6 MPa)	82.5	84.4	83.0	81.9	83.6	82.2	84.9	83.4	81.3	83.7

diameters dataset.

A jet diameter of 4 mm was identified as the optimal selection. Model 5 achieved the highest validation accuracy, reaching 98.7 %. In terms of validation loss values, Model 5 also demonstrated the lowest loss value of 4 %, surpassing the losses recorded by Model 4 at 21.7 % and Model 6 at 9.2 % (Table 6). The data presented in the graph indicate that a 4 mm aperture yields the most favorable results, confirming it as the ideal hole diameter.

Moreover, during the training process, Model 5 demonstrated slightly less oscillation in its curve than Models 4 and 6 (Fig. 6), indicating an advantage in prediction with data obtained using a 4 mm jet diameter. All three models performed excellently in testing loss values, with Model 5 achieving the highest testing accuracy of 95.3 % (Table 7). The confusion matrix results highlighted that misclassification was concentrated mainly at 93 % and 94 % moisture content, with a 3 mm diameter leading to a spread of misclassification.

Ten experiments were carried out for each of the three models, and the results are presented in Table 8. Statistical analyses were performed to compare the test accuracies of Model 5 (4 mm) with those of Model 4 (3 mm) and Model 5 (4 mm) with those of Model 6 (5 mm), aiming to assess the significance and practical differences. Normality was confirmed via Shapiro–Wilk tests for all models. Levene's test established homogeneity of variance ($p = 0.510$). A one-way ANOVA showed extremely significant performance differences among the models ($F(2,27) = 519.8$, $p < 0.001$). Post hoc Tukey HSD tests revealed significant mean differences ($p < 0.050$) between Model 5 and Model 4 (12.9) and between Model 5 and Model 6 (4.5). Cohen's d analysis indicated large effect sizes (14.3 for Model 5 vs. Model 4 and 5.4 for Model 5 vs. Model 6), highlighting substantial practical differences.

3.6. Prediction effect

From the dataset comprising 11,641 images, a subset of 3865 images, captured under 0.2 MPa and 4 mm conditions, was selected to train Models 7 and 8. These models were used to predict the moisture content of sludge samples, ranging from 79 % to 94 %, in 16 categories, with target precisions of 2 % and 1 %, respectively (Table 9).

Model 7 reached a validation accuracy of 93.5 %, whereas Model 8 achieved a validation accuracy of 87.6 %. Both models exhibited a certain decline in performance compared to Model 1 (0.2 MPa), which was trained on sludge samples with a moisture content ranging from 87 % to 94 % and an eight-category prediction, with a target precision of 1 % during optimal jet pressure selection.

During practical testing, Model 7 achieved a prediction accuracy of 86.4 %, while Model 8 attained 75.9 % accuracy in the 16-

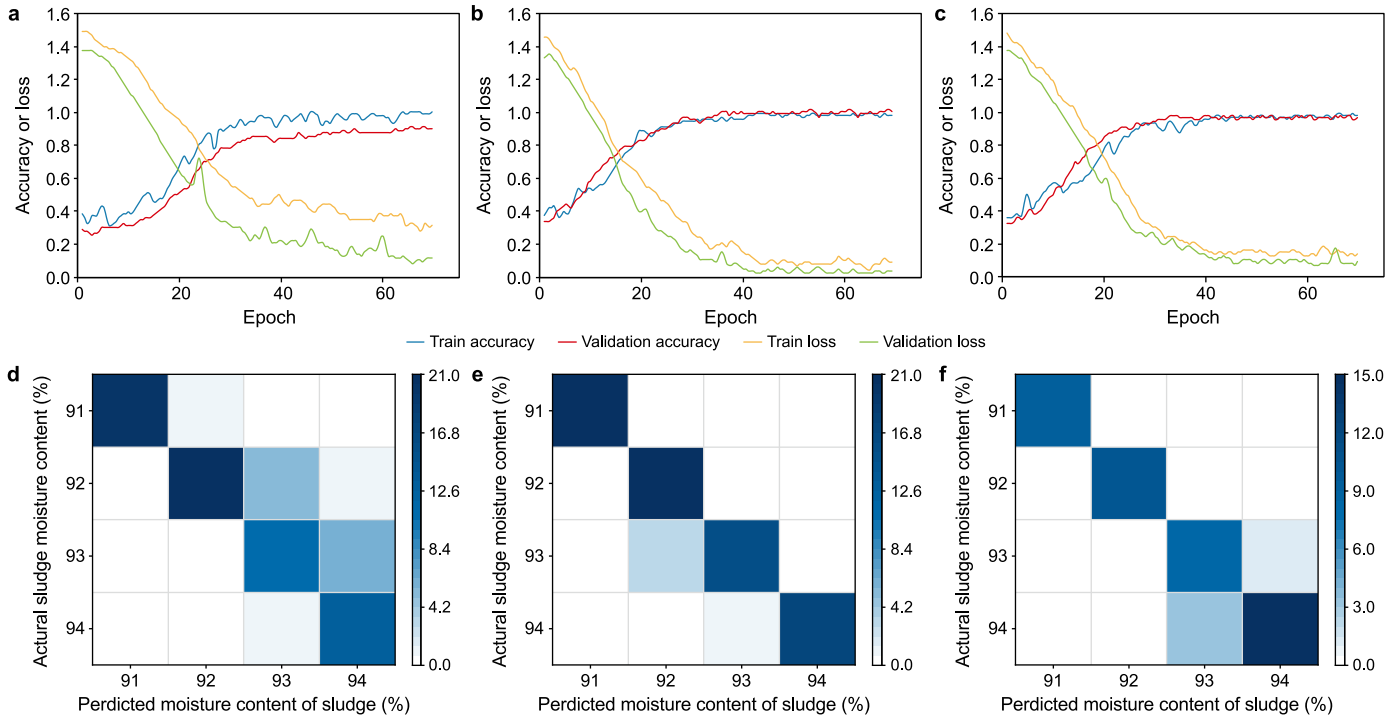

Fig. 6. a–**c,** Training process of jet feature images at different diameters: Model 4 (3 mm, **a**); Model 5 (4 mm, **b**); and Model 6 (5 mm, **c**). **d**–**f,** Confusion matrix of model predictions for jet images at different diameters: Model 4 (**d**); Model 5 (**e**); and Model 6 (**f**).

Table 7
Results from three deep learning models were compared using a dataset of 3231 sludge jet images (91–94 % moisture, 1 % gradient).

Model	Validation accuracy	Validation loss	Test accuracy
Model 4 (3 mm)	90.5 %	21.7 %	82.5 %
Model 5 (4 mm)	98.7 %	4.0 %	95.3 %
Model 6 (5 mm)	93.5 %	9.2 %	90.8 %

Table 9
Results obtained from the same dataset of 3865 sludge jet images at 79–94 % moisture content.

Model	Validation accuracy	Validation loss	Prediction accuracy
Model 7	93.5 %	19.5 %	86.4 %
Model 8	87.6 %	40.0 %	75.9 %

category prediction. Model 7 (Supplementary Table S2), with its 2 % accuracy focus, demonstrated robust prediction performance, while Model 8, targeting 1 % precision, exhibited a satisfactory level. Model 1, employed during the jet pressure selection experiment, was trained on a dataset comprising the higher moisture content range (87–94 %) utilized by Model 8 (Supplementary Table S3). However, the accuracy of Model 8 (75.9 %) was lower than that of Model 1 (96.7 %). Model 8 demonstrated a significant increase in misclassification rate in the confusion matrix, with misclassifications spreading from adjacent moisture content levels to intervals (Fig. 7). This may be due to the overlapping jet features at adjacent moisture levels caused by the different rheological properties of sludge at various moisture contents.

Expanding the moisture content range substantially increased the difficulty of learning image features for the model. Nevertheless, the moisture content prediction strategy based on sludge jet characteristics demonstrates its potential applicability.

To evaluate the generalization and prediction performance of Models 7 and 8, we conducted a five-fold cross-validation. Model 7 had an average cross-validation accuracy of 89.9 ± 1.2 % and a test set accuracy of 89.4 %. Model 8 had an average validation accuracy of 86.38 ± 2.1 % and a test set accuracy of 82.2 %. These results show that the models are stable and reliable for predicting moisture content in jet images. The confusion matrix further illustrates the models' predictive performance across categories (Fig. 8). It was observed that Model 8 was highly accurate in some categories (e.g., 79 and 80) but had confusion in others (e.g., 83 and 88), likely due to similar edge sharpness and dispersion patterns in different jet image categories. Combining the cross-validation results and

Table 8
Results of ten experimental validations for the testing accuracy of Model 4 (3 mm), Model 5 (4 mm), and Model 6 (5 mm).

Model	1	2	3	4	5	6	7	8	9	10
Model 4 (3 mm)	81.3	83.6	82.1	80.9	83.0	82.8	81.9	84.1	82.4	83.7
Model 5 (4 mm)	94.8	95.2	96.2	95.1	94.6	96.4	95.9	94.4	95.7	96.1
Model 6 (5 mm)	89.8	91.2	90.1	92.1	89.9	91.7	90.4	92.3	90.8	91.6

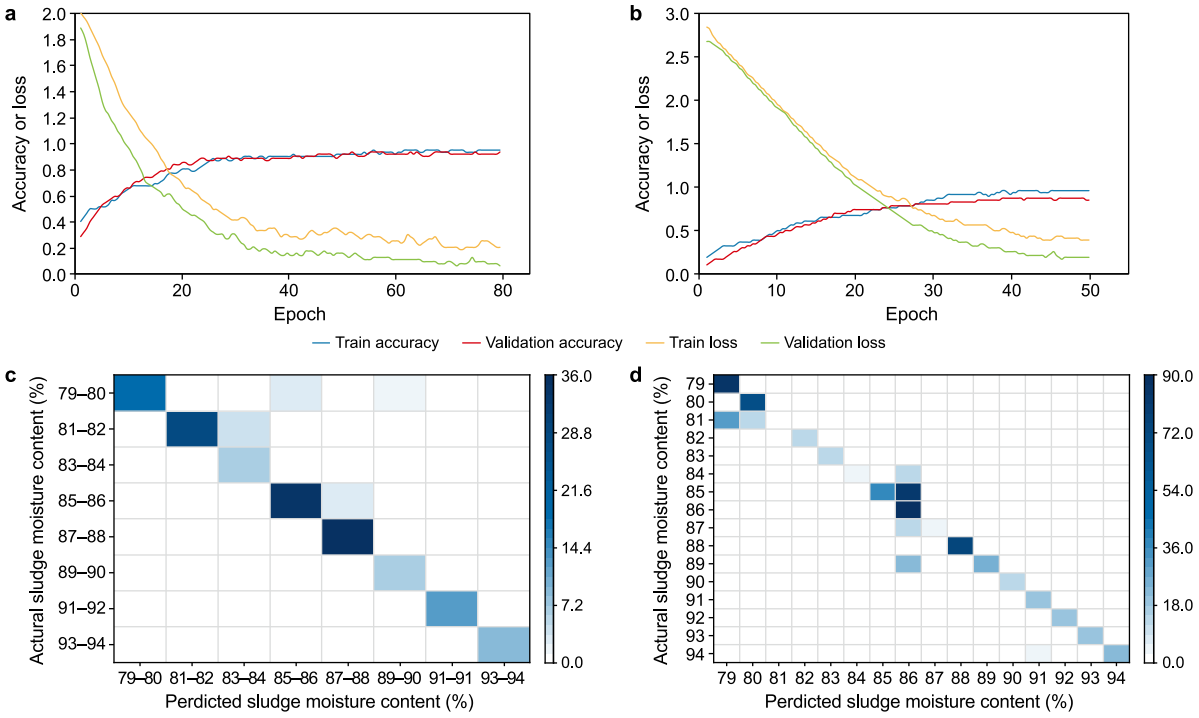

Fig. 7. a–**b,** Training process of different target accuracy: Model 7 (eight categories with a target precision of 2 %, **a**) and Model 8 (16 categories with a target precision of 1 %, **b**). **c**–**d,** Confusion Matrix of model accuracy on different moisture cut ranges: Model 7 (**c**) and Model 8 (**d**).

confusion matrix analysis, the model can effectively capture key features in jet images, but there is room for optimization to reduce misclassification. These results support the distinctiveness and practicality of the models in moisture prediction tasks.

3.7. Real-world test

We carried out moisture content predictions on dehydrated sludge samples sourced from six municipal wastewater treatment plants located in Beijing, Harbin, and Shenzhen, China. The six WWTPs were selected based on an integrated consideration of latitudinal climatic differences and diverse treatment processes, ensuring representative sludge samples from facilities across varying climatic zones and operational technologies (Fig. 9). The findings revealed that the model exhibited higher predictive accuracy in the wastewater treatment plants of Beijing and Harbin. The discrepancies between the predicted and actual moisture content of the sludge in these two regions were relatively minor. In the northern dataset, the sludge samples exhibited more consistent features, likely due to the similar conditions and treatment processes. Chemical usage in northern wastewater treatment plants is also more uniform. In contrast, Shenzhen's WWTPs have larger chemical dosage deviations, likely due to diverse demands and complex conditions. Longer transportation distances may have also affected chemical usage and the properties of the sludge. In Shenzhen, although there was a more pronounced disparity between the predicted and actual moisture content, it did not undermine the overall performance of the model. The high level of accuracy achieved by the model is chiefly ascribed to its robustness and adaptability across diverse environmental conditions. Notwithstanding the greater variability in sludge properties within the Shenzhen area, our model still manifested favorable predictive performance. This suggests that the model can furnish precise predictions, even under fluctuating circumstances.

Despite the relatively larger prediction error observed in the sewage treatment plants in Shenzhen, the model performed well in Beijing and Harbin, demonstrating great practical application potential. To further enhance the accuracy and generalization ability of the model, future research should concentrate on addressing the following issues:

(1) Standardization of sample handling and transportation. Ensuring the stability of sludge samples during transportation and minimizing the interference of external factors on test results.
(2) Model optimization and incorporation of dynamic data. Leveraging real-time sensor data or dynamic changes in the sludge treatment process to optimize the model and augment its predictive capability for complex environmental conditions.

Despite encountering certain challenges, the current model has demonstrated satisfactory results during the actual testing phase and has significant application potential. To enhance the accuracy of testing methods within the sewage treatment sector and improve the efficiency of sludge treatment and disposal, as well as the rate of resource utilization, it is imperative to further optimize both the model and the data acquisition methodologies required.

4. Conclusions

This study introduced a novel method for rapidly predicting

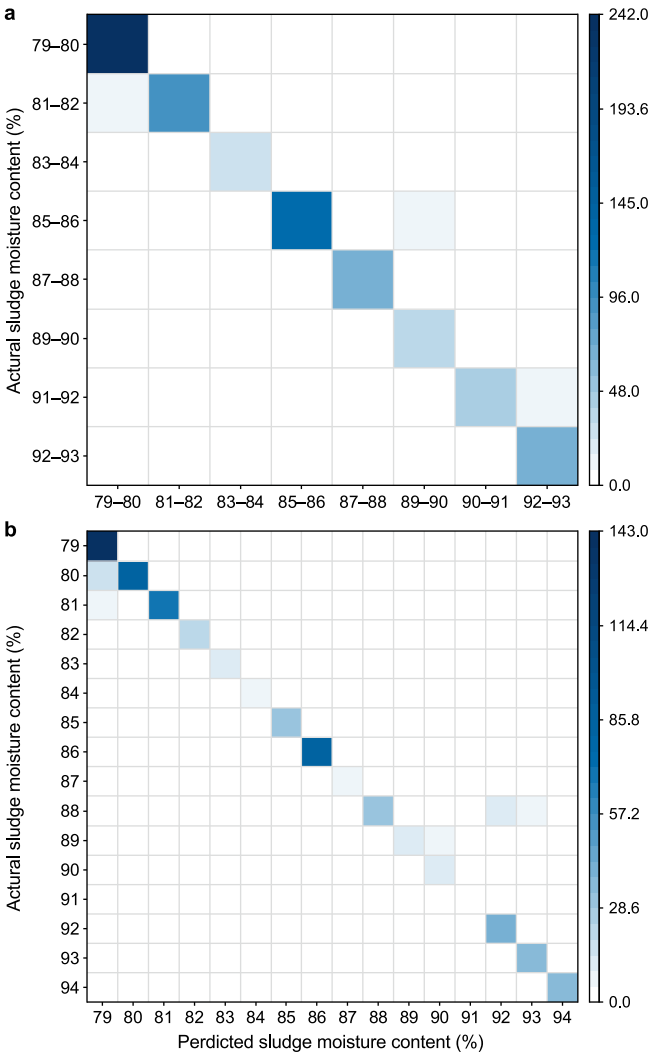

Fig. 8. Confusion matrix of the model prediction capability of Model 7 (eight categories with a target precision of 2 %, **a**) and Model 8 (16 categories with a target precision of 1 %, **b**).

sludge moisture content based on jet characteristic images, reducing the testing time to under 20 s. By constructing the instantaneous capturing of activated sludge jet expansion images (iCASJEI) system to obtain characteristic sludge jet image data and combining it with CNN for moisture content prediction, we compared and validated the predictive performance of different models under varying experimental conditions using dewatered sludge from sewage treatment plants. The key findings are as follows:

(1) The entire apparatus or system is capable of efficiently predicting the moisture content of sludge. It achieved a prediction accuracy of 86.4 % for eight categories (2 % precision) and 75.9 % for sixteen categories (1 % precision). This system demonstrates excellent performance across sludge samples from various cities.
(2) The most effective extraction of sludge jet characteristics was achieved with a jet pressure of 0.2 MPa and a jet nozzle diameter of 4 mm. Model performance analysis under these conditions indicated an optimal prediction of moisture content.
(3) We compared the predictive performance of VGG-16, AlexNet, and LeNet CNNs on images of sludge jets. VGG-16 demonstrated superior performance.
(4) In the future, we plan to obtain more samples to enhance accuracy, focus on additional sludge indicators, and conduct research on non-Newtonian fluids, aiming to give this technology some generalizability.

This study confirms the potential of moisture content detection methods based on the non-Newtonian fluid properties of sludge, which have a faster testing speed than traditional methods and yield promising prediction results. This study functions solely as an initial validation; therefore, the sample must be enlarged to include extreme rheological conditions. This process will include expanding the capacity of the image dataset, refining the model, and performing multiple simultaneous jet calibrations to improve the accuracy of the method.

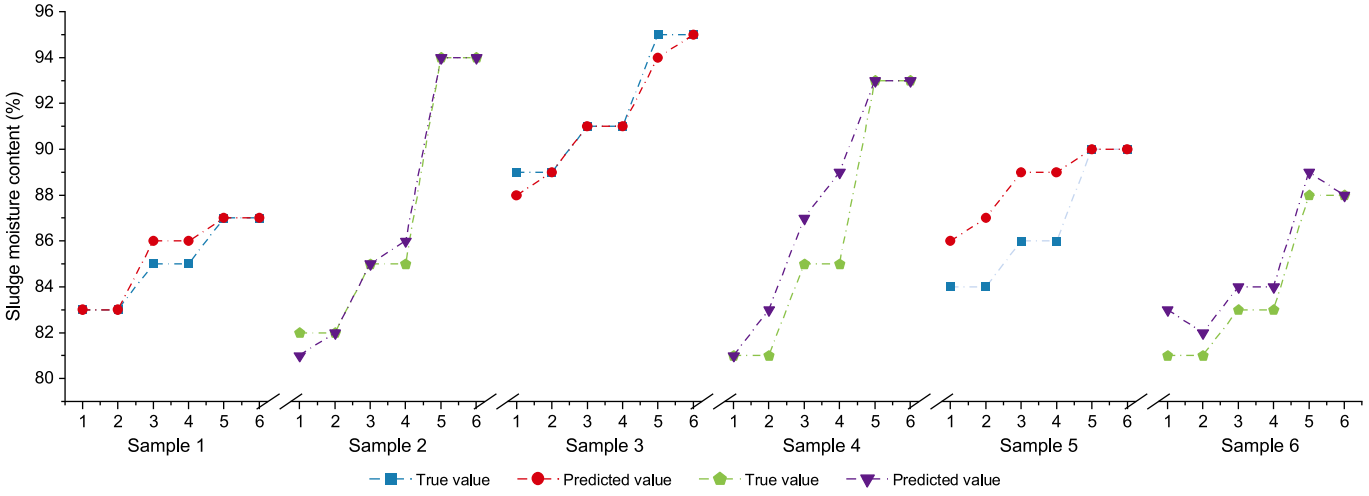

Fig. 9. Practical tests using six samples obtained from wastewater treatment plants located in Daoxiangcun, Beijing; Harbin bungalow; Huadu, Beijing; Binhe, Shenzhen; Buji, Shenzhen; and Xili, Shenzhen.

CRediT authorship contribution statement

Tiefu Xu: Resources, Project administration, Conceptualization. **Bo Zhang:** Validation, Data curation. **Yue Sun:** Software, Conceptualization. **Man Wang:** Writing – original draft, Conceptualization. **Yuejia Chen:** Validation, Data curation. **Penghe Zhu:** Validation, Data curation. **Binqiao Ren:** Validation, Data curation. **Yanhong Jie:** Software. **Guotao Wang:** Supervision, Methodology, Conceptualization.

Declaration of competing interest

The authors declare that they have no known competing financial interests or personal relationships that could have appeared to influence the work reported in this paper.

Acknowledgements

This work was supported by Heilongjiang Provincial Natural Science Foundation of China (LH2024E111); the Higher Education Institutions' Collaborative Innovation Achievement Project of Heilongjiang Province (LJGXCG2023-077, LJGXCG2024-P08), Outstanding Youth Science Fund of Heilongjiang University for the Year 2022 (JCL202204); Special Fund Project of Heilongjiang University (2023-KYYWF-1433).

Appendix A. Supplementary data

Supplementary data to this article can be found online at https://doi.org/10.1016/j.ese.2025.100614.

References

[1] M. Liu, S. Rashid, W. Wang, et al., The application of chitosan quaternary ammonium salt to replace polymeric aluminum ferric chloride for sewage sludge dewatering, Water Res. (2024) 121539.
[2] Farokh Laqa Kakar, Frew Tadesse, Elsayed Elbeshbishy, Comprehensive review of hydrothermal pretreatment parameters affecting fermentation and anaerobic digestion of municipal sludge, Processes 10 (2022) 2518.
[3] Zeyu Li, Hongbo Chen, Elucidating the role of solids content in low-temperature thermal hydrolysis and anaerobic digestion of sewage sludge, Bioresour. Technol. 362 (2022) 127859.
[4] Eva Kocbek, Hector A. Garcia, Christine M. Hooijmans, et al., Effects of the sludge physical-chemical properties on its microwave drying performance, Sci. Total Environ. 828 (2022) 154142.
[5] Jiefu Wang, et al., Unblocking the rate-limiting step of the municipal sludge anaerobic digestion, Water Environ. Res. 94 (2022).
[6] S.N. Zailani, et al., Compost physical properties study on degradation of poultry manure composting in closed-aerated composter, IOP Conf. Ser. Mater. Sci. Eng. 932 (1) (2020) 012012, 8pp.
[7] Jie Qin, Xiaoyong Fu, Xuemin Chen, et al., Changes in physicochemical properties and microfauna community during vermicomposting of municipal sludge under different moisture conditions, Environ. Sci. Pollut. Res. 28 (24) (2021) 31539–31548.
[8] Qunxing Huang, Ben Yu, Ben Yu, et al., Effect of moisture on sewage sludge combustion temperature profile and heavy metal leaching, Dry. Technol. 34 (15) (2016) 1810–1819.
[9] J. Zhang, P. Gan, T. Xie, Y. Liu, H. Zhu, Impacts of wet thermal treatment on heavy metals speciation in contaminated waste activated sludge using a modified sequential extraction scheme, Bioresources 17 (2) (2022) 2116–2128.
[10] Beiping Zhang, Sijiang Xiong, Bo Xiao, et al., Mechanism of wet sewage sludge pyrolysis in a tubular furnace, Int. J. Hydrogen Energy 36 (2011) 355–363.
[11] H. Zhang, W. Tao, M. Hou, et al., Effect of potassium ferrate as a dewatering conditioner on sludge pyrolysis characteristics and the releasing characteristics of nitrogen, sulfur, and chlorine during sewage sludge pyrolysis, Processes 11 (3) (2023).
[12] Jaroslav Moško, Michal Jeremiáš, Siarhei Skoblia, et al., Residual moisture in the sewage sludge feed significantly affects the pyrolysis process: simulation of continuous process in a batch reactor, J. Anal. Appl. Pyrolysis 161 (2022) 105387.
[13] Cesar Huiliñir, Manuel Villegas, Simultaneous effect of initial moisture content and airflow rate on biodrying of sewage sludge, Water Res. 82 (2015) 118–128.
[14] M.C. Collivignarelli, M. Carnevale Miino, S. Bellazzi, et al., Review of rheological behaviour of sewage sludge and its importance in the management of wastewater treatment plants, Water Pract. Technol. (1) (2022) 17.
[15] B. VURAL, S. COSKUN, Relations among sludge rheological properties and operational problems in an industrial zone wastewater treatment plant, Int. J. Progressive Sci. Technol. 34 (1) (2022) 320.
[16] Hélène Caillet, L. Adelard, A review on the rheological behavior of organic waste for CFD modeling of flows in anaerobic reactors, Waste and Biomass Valorization (2022) 1–17.
[17] C.P. C, D.J. Lee, Moisture distribution in sludge: effects of polymer conditioning, J. Environ. Eng. 125 (1999) 340–345.
[18] Minh Chien Vu, Tomoaki Satomi, Hiroshi Takahashi, Influence of initial water, moisture, and geopolymer content on geopolymer modified sludge, Constr. Build. Mater. 235 (2020) 117420.
[19] Osei Asafu-Adjaye, Brian Via, Bhima Sastri, et al., Displacement dewatering of sludge with supercritical CO2, Water Res. 190 (2021) 116764.
[20] Cai Lu, Tong-Bin Chen, Ding Gao, et al., Time domain reflectometry measured moisture content of sewage sludge compost across temperatures, Waste Manag. 33 (1) (2013) 12–17.
[21] Cai Lu, Ding Gao, Nian Hong, Measurement of moisture content using time domain reflectometry during the biodrying of sewage sludge with high electrical conductivity, Dry. Technol. 35 (1) (2017) 108–115.
[22] Huazhen Mao, Fei Wang, Feiyan Mao, et al., Measurement of water content and moisture distribution in sludge by 1H nuclear magnetic resonance spectroscop, Dry. Technol. 34 (3) (2016) 267–274.
[23] Binqi Rao, Hongru Pang, Feibiao Fan, et al., Pore-scale model and dewatering performance of municipal sludge by ultrahigh pressurized electro-dewatering with constant voltage gradient, Water Res. 189 (2021) 116611.
[24] Ya-Li Zhang, Ping Sun, Bing-Bing Dai, What affects the accuracy and applicability of determining wastewater sludge water content via low-field nuclear magnetic resonance? Environ. Res. 226 (2023) 115702.
[25] Nicky Eshtiaghi, Flora Markis, DongYap Shao, et al., Rheological characterisation of municipal sludge: a review, Water Res. 47 (15) (2013) 5493–5510.
[26] Kevin Hii, Raj Parthasarathy, Saeid Baroutian, et al., Rheological measurements as a tool for monitoring the performance of high pressure and high temperature treatment of sewage sludge, Water Res. 114 (2017) 254–263.
[27] Jean-Christophe Baudez, About peak and loop in sludge rheograms, J. Environ. Manag. 78 (3) (2006) 232–239.
[28] Jiankai Jiang, Jing Wu, Souhila Poncin, et al., Rheological characterization of digested sludge by solid sphere impact, Bioresour. Technol. 218 (2016) 301–306.
[29] D. Stickland Anthony, Compressional rheology: a tool for understanding compressibility effects in sludge dewatering, Water Res. 82 (1) (2015) 37–46.
[30] Hou-Feng Wang, Ya-Nan Bai, Wei Zhang, et al., Supplementary In-Depth analysis of the waste activated sludge dewatering process using a rheological analysis, ACS ES&;T Eng. 1 (2) (2021) 289–297.
[31] Boran Wu, Donghai Yang, Ningrui Yu, et al., A quantitative theory integrating solid surface hydrophilicity and pore structure features for non-phase-change drying of sewage sludge through gradient increase of ultrahigh filtration pressure, Water Res. 247 (2023) 120765.
[32] Li Ji, Hao Xiaodi, Zhan Shen, Low-temperature drying of waste activated sludge enhanced by agricultural biomass towards self-supporting incineration, Sci. Total Environ. 888 (2023) 164200.
[33] Gang Zhao, Bo Pang, Zongxue Xu, et al., Urban flood susceptibility assessment based on convolutional neural networks, J. Hydrol. 590 (2020) 125235.
[34] ChengJun Guo, YaLan Xu, Tian Zhong, Inversion of PM2.5 atmospheric refractivity profile based on AlexNet model from the perspective of electromagnetic wave propagation, Environ. Sci. Pollut. Control Ser. 27 (2020) 37333–37346.
[35] W.C. YEH, C.Y. KUO, J.M. CHEN, et al., Pioneering data processing for convolutional neural networks to enhance the diagnostic accuracy of traditional chinese medicine pulse diagnosis for diabetes, Bioengineering 11 (6) (2024) 561.
[36] Haoyan Yang, Jiangong Ni, Jiyue Gao, et al., A novel method for peanut variety identification and classification by improved VGG16, Sci. Rep. 11 (1) (2021) 15756.
[37] A. Khan, T. Rahman, M.Z. Islam, et al., An approach for classification of alzheimer's disease using deep neural network and brain magnetic resonance imaging (MRI), Sci. Rep. 14 (3) (2024) 1234–1245.
[38] S.M. Hamylton, R.H. Morris, R.C. Carvalho, et al., Evaluating techniques for mapping island vegetation from unmanned aerial vehicle (UAV) images: pixel classification, visual interpretation and machine learning approaches, Int. J. Appl. Earth Obs. Geoinf. 89 (2020) 102085.
[39] S. Kumar, H. Wang, R. Gupta, et al., Competitive deep learning methods for COVID-19 detection using X-ray images, BMC Med. Imag. 21 (1) (2021) 1–14.

[40] .
[41] PaddlePaddle, PaddlePaddle - an open source deep learning platform rooted in industrial practice, Online (2023). Available at: https://www.paddlepaddle.org.cn/.
[42] Matplotlib, Matplotlib -Visualization with Python [Online]. Available at: https://matplotlib.org/, 2024.
[43] NumPy, NumPy - [Online]. Available at: https://numpy.org/, 2024.
[44] Pandas, Pandas - Python data analysis library [Online]. Available at: https://pandas.pydata.org/, 2024.
[45] Ehsan Farno, Jean Christophe Baudez, Rajarathinam Parthasarathy, et al., Rheological characterisation of thermally-treated anaerobic digested sludge: impact of temperature and thermal history, Water Res. 56 (2014) 156–161.
[46] C. Ségalen, E. Dieudé-Fauvel, J.C. Baudez, Electrical and rheological properties of sewage sludge – impact of the solid content, Water Res. 82 (2015) 25–36.
[47] Jizhao Liang, Melt die-swell behavior of polyoxymethylene blended with ethylene-vinyl acetate copolymer and high-density polyethylene, Polym. Test. 68 (2018) 213–218.